



## **Brief communication: Remotely piloted aircraft systems for rapid emergency response: road exposure to rockfall in Villanova di Accumoli (Central Italy)**

Michele Santangelo<sup>1</sup>, Massimiliano Alvioli<sup>1</sup>, Marco Baldo<sup>2</sup>, Mauro Cardinali<sup>1</sup>, Daniele Giordan<sup>2</sup>, Fausto Guzzetti<sup>1</sup>, Ivan Marchesini<sup>1</sup>, and Paola Reichenbach<sup>1</sup>

<sup>1</sup>Consiglio Nazionale delle Ricerche, Istituto di Ricerca per la Protezione Idrogeologica, via Madonna alta 126, 06128 Perugia, Italy

<sup>2</sup>Consiglio Nazionale delle Ricerche - Istituto di Ricerca per la Protezione Idrogeologica, 10135, Torino, Italy

**Correspondence:** Michele Santangelo ([michele.santangelo@irpi.cnr.it](mailto:michele.santangelo@irpi.cnr.it))



**Abstract.** The use of Remotely Piloted Aircraft Systems (RPASs) in geosciences is often aimed at the acquisition of an image sequence to produce digital models and orthophotographs of the topographic surface. The technology can be applied for rockfall hazard and risk assessment. To study rockfalls, an approach consists in the application of numerical models for the computation of rockfall trajectories. Data required for such models include accurate digital terrain models, location of the instability source areas, and the mechanical properties of the terrain. In this article, we present an analysis of the earthquake-triggered rockfall that occurred along the SP18 in Villanova di Accumoli (Lazio, central Italy) during the 24 August 2016 seismic sequence. A survey with a multicopter was carried out to obtain an accurate surface model of the terrain, the identification and characterization of the source areas and of other instable blocks in areas not accessible in the field. The investigated area extends for 6,500 m<sup>2</sup> and was covered by 161 photographs that were used to obtain an orthophoto with a ground resolution of 2.5 cm, and a digital surface model with a ground resolution of 20 cm × 20 cm which was processed and fused with GNSS RTK data. We run the numerical model STONE, using the source areas mapped in the field and adopting a slope threshold to get a map showing the rockfall potential trajectories. Results showed that only the part of the road SP18 hit by the rockfall was exposed to further rockfall impacts. In particular, it was observed that 16% (i.e. 5,108) of the 31,800 simulated trajectories reached or crossed this tract of the road. Based on these data, limited protection measures were suggested. The combined use of RPAS data, fused with ground GPS points, an accurate geomorphological survey, and terrain static and dynamic parameters from the literature, allows fast, low-cost and replicable numerical modelling for emergency response and adoption of proper protection measures.

## 1 Introduction

Rockfall is a widespread natural hazard that poses continuous risk to the population in mountain areas worldwide (Whalley W, 1984; Guzzetti et al., 2002). Due to the prevalent type of movement (free falling, bouncing, rolling, sliding), rockfalls are among the fastest and deadliest landslide type (Evans S, 1997; Guzzetti et al., 2002). Rockfalls can be triggered by earthquakes, intense rainfall, frost weathering, wind and roots growth, and even traffic (Guzzetti et al., 2004). The elements at risk most exposed to rockfall hazard are transport corridors (Guzzetti et al., 2002; Budetta, 2004; Guzzetti et al., 2004), which often cross hazardous areas. In particular, rockfalls cause relevant damages to structures and infrastructures along secondary and minor transport networks, where adequate protection measures are not economically sustainable (Corominas et al., 2005; Ferlisi et al., 2012), and pose severe risk to people.

During triggering events such as seismic sequences, areas exposed to rockfall hazard can be hit in several places (Guzzetti et al., 2004), causing multiple damages and interruptions of the infrastructures, particularly roads and rails. In such events, it is important to characterize the most critical situations along roads and rails to guarantee, in short time spans, a safe use of the transportation infrastructures. Operating workflows to better characterize rockfall source areas and trajectories could lead to identify areas where rockfalls can interact with roads, allowing for tailored protection measures, and developing more rapid infrastructure protection activities.

Defining the potential interaction of rockfalls, known the geographic location of elements at risk, is a challenging task. Empirical, process-based and GIS-based software including e.g., ILWIS (van Dijke and van Westen, 1990), STONE (Guzzetti



et al., 2002), HY-STONE (Agliardi and Crosta, 2003), CONEFALL (Jaboyedoff and Labiouse, 2011), Rockyfor3D (Luuk Dorren, 2015), have been implemented and used to model the spatial pattern of rockfalls trajectories. All the modelling approaches are based on at least a given distribution of rockfall source areas, and a digital elevation model (DEM). Detection and mapping of unstable rock-masses can be accomplished by field activities, interpretation of high and very high-resolution images and DEMs, or using morphometric criteria (Michoud et al., 2012). Depending on the scale of the modelling, elevation data can be coarse to very fine. For example, for regional scale modelling, a ground sampling distance (GSD) of 25 m (Guzzetti, 2003)<sup>1</sup> or 10 m is adequate (Guzzetti et al., 2003), whereas very high resolution elevation data (GSD of 1 m or less) are suitable for slope scale models.

High and very high resolution elevation data can be successfully acquired using cameras mounted on Remotely Piloted Aircraft Systems (RPAS). The acquired high(ultra)-resolution images with different orientations of the camera (nadir, oblique) can be used to obtain elevation data through the application of Structure from Motion algorithms (SfM) (Westoby et al., 2012; Nex and Remondino, 2014). SfM is a photogrammetric-range imaging technique capable of finding homologue points in a sequence of images acquired with a high overlap, and to transform the homologue points in a georeferenced cloud of elevation points (Turner et al., 2012). The accuracy of the positioning of SfM products can be improved using Ground Control Points (GCPs) whose position is measured using e.g., GNSS (Global Navigation Satellite System) systems (Nex and Remondino, 2014). The main products of RPAS photogrammetry that can support the study of rockfalls are Digital Surface Models (DSMs), and true orthophotographs (Giordan et al., 2018). High resolution elevation data can also be collected by aerial laser scanners (LiDAR), which acquire a set of measures of distance between the laser scanner and the ground surface (Razak et al., 2013).

Both LiDAR and SfM have advantages and limitations. In particular, LiDAR is considered a better solution for densely vegetated areas (Razak et al., 2013) where photogrammetric techniques are more limited in obtaining ground elevation data. On the other hand, aerial LiDAR is not effective for the characterization of sub-vertical slopes, and rock cliffs, where the acquisition of oblique photo-sequences is the best solution for a more detailed representation of rockfall source areas (Giordan et al., 2015a). Use of RPAS for SfM is a solution that requires limited costs and mission planning and setup time compared to LiDAR, particularly if the study area is small (up to few square kilometres). Such advantages can be important particularly where a multi temporal approach has to be adopted to detect the evolution of the studied area (Fiorucci et al., 2018) or during emergencies, where support to decision makers for the identification and planning of first responses must be provided shortly (Giordan et al., 2015b).

In particular, the use of RPAS can be effective for a fast response to natural disasters (Chou et al., 2010; Ezequiel et al., 2014; Xu et al., 2014; Boccardo et al., 2015; Liu et al., 2015; Huang et al., 2017). According to Giordan et al. (2015a), two approaches can be adopted for the use of RPAS depending on the slopes steepness. For steep slopes, it is recommended the use of multi-rotors RPAS which allow to acquire oblique photographic-sequences. On the contrary, on gentle slopes nadir acquisition done by fixed wings RPAS can be considered the best solution to obtain a high-resolution coverage of large areas. In the study of rockfall affected areas, a hybrid approach can be considered for the acquisition of a DSM that can be used for the definition of rock blocks trajectories and the study and characterization of source areas. Furthermore, RPAS guarantees

<sup>1</sup>[http://damocles.irpi.cnr.it/docs/final\\_reports/Perugia-Detailed-Report-Feb2001-Mar2003.pdf](http://damocles.irpi.cnr.it/docs/final_reports/Perugia-Detailed-Report-Feb2001-Mar2003.pdf)



the possibility of acquiring high resolution DTMs also in inaccessible areas (Obanawa, H. Hayakawa, Y. and Gomez, 2014). Several examples of the use of RPAS for the acquisition of oblique (Salvini et al., 2016, 2018; Giordan et al., 2015b; Török et al., 2018; Huang et al., 2017) and nadiral image sequences (Saroglou et al., 2018) for the study identification of rock slopes instabilities have been published in recent years.

5 Despite such an increasing attention on applications of RPAS images and photogrammetry to landslides risk assessment, only a limited number of articles focuses on applications during emergencies (Chou et al., 2010; Boccoardo et al., 2015; Liu et al., 2015; Huang et al., 2017) and on the assessment of the extent of damages caused by natural disasters. Furthermore, none of them, to the best of our knowledge, focuses on testing a procedure that guarantees semi-quantitative information in a relatively short time to provide an evaluation of the residual rockfall risk during emergencies, when time and budget constraints  
10 are restrictive.

In this paper, we describe the use of RPAS to study an earthquake-triggered rockfall in the vicinity of the Villanova di Accumoli, Rieti, central Italy. The seismic sequence that started on 24 August 2016 struck central Italy triggering numerous rockfalls that caused damage to roads. Provincial road SP18 near Villanova di Accumoli was closed after a 1 m<sup>3</sup> boulder fell from a rock cliff and crossed the Provincial road (Fig. 1). During the seismic emergency, the Italian National Department  
15 of Civil Protection was supported by the Research Institute for Geo-Hydrological protection of the Italian National Research Council (CNR-IRPI) in the definition of the conditions to safely reopen the road. To answer the request, a numerical model was applied to the remaining instable rock masses to evaluate possible rockfall trajectories, and to define locations where the road was exposed to rockfall hazard.

## 2 Study area

20 The study area is located close to the village of Villanova di Accumoli, in the Accumoli municipality, central Italy (Fig. 1A). In the area, the main vulnerable element subject to rockfalls was a portion of the SP18 road connecting Villanova di Accumoli to the San Giovanni village (Fig. 1A).

[FIGURE 1]

The area consisted of a rocky hillslope from which rockfalls detached, reaching the SP18 road (Fig. 1A). Visual interpretation  
25 of stereoscopic black and white aerial photographs taken in 1954 at 1:33,000 scale revealed that the cliff from where the rockfall originated is part of a partially dismantled scarp of a deep-seated, disrupted rockslide (Fig. 1B). Additional visual interpretation of stereoscopic colour aerial photographs taken in 1977 at 1:13,000 scale revealed that the main landslide rocky escarpment is characterized by two areas that underwent progressive retreat, forming three cone-shaped, convex, sparsely vegetated talus deposits (Fig. 1B). Further analysis of the two sets of aerial photographs revealed that in the central part of the escarpment  
30 the talus deposit was mined and partly removed between 1954 and 1977 (Fig. 1B). Outside of the talus deposits, the landslide scarp shows an average slope of around 40°, it is mainly bare and bedrock crops out. At the base of the slope, the top of the landslide deposit is covered partially by talus that supports a dense deciduous wood.



In the study area, a regional thrust brings the carbonatic units of the Umbria-Marche stratigraphic sequence over the Laga Formation (Cacciuni et al., 1995). The boulders that hit the SP18, and the majority of the boulders found on the talus slope above the SP18 road, belong to the Maiolica Fm., a layered and highly fractured mudstone, upper Jurassic to lower Cretaceous in age.

5 In the following, we describe the two rockfall source areas, shown as “site 1” (S1) and “site 2” (S2) in Fig. 1A,C, recognized during the field survey.

Site 1 (S1 in Fig. 1C,D) is a 30 m high cliff in fractured limestone 110 m NE from the road. The talus downhill of the cliff has an average slope of about 31°. It was partly mined in the 1950s, and in the mined area, the average slope is 40°. Moving from the source area to the road, the slope shows a decreasing inclination. For a distance of 50 m uphill of the road, a system of scarps, counter scarps and rough and ruined embankments parallel to the SP18 was developed to protect the road during the mining activities that removed a large part of the original talus. The quarry protection system is now completely wooded. From S1, the boulders moved primarily along ballistic trajectories (“free fall”) as demonstrated by the impact points found on the ground and the scars left on the tree trunks. At impact points on bedrock and talus, the fallen blocks broke up in pieces, the larger of which 0.25 – 0.30 m<sup>3</sup> in volume, were found on the nearly flat area uphill of the road. Analysis of the scars left by the falling blocks on the trees revealed that the rockfall trajectories did not exceed an elevation above the local terrain of about 1.5 m. Based on the boulders found in the field, the area enclosing the trajectories of the rockfalls detached from S1 extends for about 4,000 m<sup>2</sup>. Using the DSM and the orthophoto obtained through SfM, it was possible to estimate the total volume of the rocks detached in 7.5 m<sup>3</sup>. Based on the evidence of the fracturing of the remaining unstable rock mass, it is possible to hypothesize that the initial detached rock mass consisted of few large boulders that then further fragmented. The rocky material detaching from S1 did not reach the SP18, but stopped on the talus deposit and on the quarry protection system. Visual analysis of the photographs taken by the RPAS (Fig. 2D) allowed identifying several unstable rock blocks present in the vicinity of S1. Such rock blocks were separated from the bedrock by open fractures, which could be further enlarged due to intense rainfall and by frost and thaw cycles, not infrequent in the area. The overall volume of the unstable blocks was estimated in the range 30 - 50 m<sup>3</sup> by combining a GIS measure of the area recognized on the orthophoto (10 m<sup>2</sup>) and field observation, where the height of the unstable rock blocks was estimated spanning between 3 and 5 m.

Site 2 (S2 in Fig. 1C) is located along a slope covered by a talus deposit, with a mean slope angle of about 32°. From S2, a 1 m<sup>3</sup> boulder detached and reached the SP18 road (Fig. 1C, E). The analysis of the boulder impact points on the road (Fig. 1E) and its final position allowed us to reconstruct the boulder trajectory, from 70-90 m uphill of the road, where we were able to identify the most likely source area (Fig. 1A, C). Along the hillslope of S2, six boulders of similar size were found on the talus deposit. It is possible that the seismic activity worsened the stability conditions of the boulders, increasing the rockfall hazard along the road.

Analysis of the distribution of the rockfall impact points and of the trees scars revealed that the height of the trajectory of the 1 m<sup>3</sup> boulder never exceeded one meter above the ground. The boulder did not break along its path, and stopped 15 m downslope of the SP18.



### 3 Methods

#### 3.1 Elevation data acquisition

Numerical modelling of rockfalls requires the availability of an accurate digital model of the topographic surface. For the purpose, we performed a dedicated RPAS image sequence acquisition using a SenseFly® Albris® multicopter equipped with a 34 Mpixels RGB camera and an on board GNSS system for the accurate geolocation of the acquired images. A total 161 nadir photographs with a frontal overlap of 75% and a side overlap of 60% were taken at an altitude of 90 m above the ground (Fig. 1F). The altitude above the ground was set up using the dedicated mission planner using the SRTM DTM (Farr et al., 2007) for reference. Keeping constant the elevation of the flight with respect to the ground guaranteed a homogeneous GSD (ground sample distance) across the study area. The resulting photographs cover an area of about 65,000 m<sup>2</sup> with a GSD of about 1.5 cm × 1.5 cm. Using this ultra-resolution photographic sequence, we prepared an orthophotograph of the entire study area with a nominal ground resolution of about 2.5 cm × 2.5 cm, and a Digital Surface Model (DSM) with a nominal ground resolution of about 20 cm × 20 cm.

#### 3.2 Structure From Motion applied to RPAS ultra-resolution images

We processed the collected images using Agisoft Photoscan® software<sup>2</sup> and produced the true orthophotograph (OP) and the DSM. A total of 10 GCPs were used to improve the accuracy of the geographic positioning of the DSM and the OP. GCPs consisted in 40 cm × 40 cm targets. The positioning accuracy of the resulting DSM and true orthophotograph was evaluated using 70 additional CPs. The geographical coordinates of both GCPs and CPs were obtained using a GNSS RTK VRS (Global Navigation Satellite System, Real Time Kinematic, Virtual Reference Station) positioning technique. The estimated planimetric-altimetric accuracy of the absolute positioning of the GCPs and CPs was about 10 cm.

To produce a DTM, the fingerprint of vegetation and other elements that could hide the ground were filtered out. For the purpose, we first used a geometric and a radiometric filter available in Photoscan®. Next, we performed a manual cleaning of the terrain elevation data. After the cleaning, Photoscan® was used to interpolate the remaining ground points. In some sectors, the interpolation was based on a very limited number of data points due to the coverage of trees, which resulted in an over-smoothed DTM (Fig. 2A).

#### 3.3 GNSS RTK VRS elevation data integration

In the areas where the elevation information was unavailable (due to the presence of trees), we obtained additional elevation information with a GNSS survey, applying an RTK VRS correction. For the purpose, we used a Leica® Zeno 20<sup>3</sup> device in conjunction with an Android smartphone with GPRS connection for the real-time correction of the positioning (RTK VRS). We acquired a total of 73 points (Fig. 2A), corresponding to an average density of one point every 100 m<sup>2</sup> (i.e., a GSD of approximately 10 m) with a nominal positional accuracy of less than one meter.

<sup>2</sup><http://www.agisoft.com>

<sup>3</sup><https://leica-geosystems.com/>



To obtain a continuous DTM covering the entire study area, we merged the two elevation data sets obtained from the aerial and the ground-based surveys. For the purpose, a mask of the wooded area was drawn in the GIS, and a 5-m external buffer was applied to enclose in the area a 5-meter wide band containing elevation data from the DTM generated by SfM. Elevation data contained in the buffer were then included in the interpolation of the 73 GNSS RTK VRS data points using the linear  
5 Delaunay interpolation method available in the v.surf.nmbathy GRASS GIS tool (GRASS Development Team, 2017). Using the elevation data available in the buffer guaranteed that no “step-like” features occurred at the junction between the original DTM and the DTM obtained by the GNSS-RTK VRS survey in the wooded area (Fig. 2B). The GSD of the merged DTM was set to 1 m, the highest resolution handled by the rockfall modelling software STONE (Guzzetti et al., 2002).

We stress that the DTM accuracy is not uniform over the entire study area. The information is denser and more accurate in  
10 unwooded areas, where the elevation was obtained by the SfM, as opposed to areas where data were collected by the GNSS survey. Despite the information under the tree canopies is less dense than in the rest of the area, the GNSS points were acquired to best represent the ground morphology.

[FIGURE 2]

### 3.4 Numerical modeling of rockfalls

15 Numerical modelling of rockfall was performed using STONE, a software for the 3-D, kinematical simulation of rockfalls (Guzzetti et al., 2002). STONE simulates the fall of a boulder along a slope within a three-dimensional approach, considering the moving boulder dimensionless and with all the mass concentrated in the centre of mass, and computing the trajectory at discrete time steps. Within each time step, the boulder can be in one of three “states” i.e., free fall, rolling, or bouncing. The trajectory of a boulder is computed automatically from the DTM, and it depends on the starting point, the topography, and the  
20 coefficients used to simulate the loss of velocity at the impact points or during the rolling state. The coefficients can be obtained from existing thematic data, or estimated analysing geological, geomorphological and land cover maps. For each simulation, and for each simulated trajectory, the program allows a random variation of the coefficients and of initial direction of motion, resulting in an output with probabilistic content. The minimal input required to perform a simulation with STONE consists of three raster maps, containing: (i) elevation information (i.e., the DTM); (ii) the location of the rockfall detachment areas  
25 (source grid cells), also describing the number of rockfall trajectories (falling blocks) to be simulated for each grid cell in the source areas; (iii) values of the parameters describing the tangential and the normal energy restitution at each impact point, for each grid cell; (iv) values of the parameter used to describe the dynamical friction coefficient where the rockfall is rolling, for each grid cell; (v) values of the initial rockfall velocity, for each simulated trajectory. Additional inputs and available options are described in (Guzzetti et al., 2002).

30 The output of the software consists of three raster maps (Guzzetti et al., 2002) in which, for each grid cell, the following information is given: (i) the number of modelled rockfall trajectories crossing the cell, (ii) the maximum velocity of the simulated rockfalls crossing the cell, and (iii) the maximum height reached by the simulated rockfalls passing through the cell. The three quantities can be used to evaluate rockfall hazard in each DTM cell (Guzzetti et al., 2003, 2004). In particular, we considered the grid showing the count of the simulated rockfall trajectories as a proxy for the probability that a given grid



cell is affected by a rockfall. The larger the number of trajectories, the larger the expected likelihood of rockfall occurrence in a given cell. The grids containing the maximum velocity and height of the possible rockfall were not used in this work. Analysis of the map of the trajectories allows to distinguish segments of the road that are predicted to be safe from the ones with a non-negligible probability to be hit by a rockfall, within the STONE model. Based on field observations, the possible source areas were singled out by selecting cells with slope steeper than  $60^\circ$ . In addition, we considered as source areas also the locations of the rockfall sources observed in the field, using a circular 1 m buffer around the surveyed point locations.

Assigning the values of energy restitution and dynamic friction parameters required by the STONE model is a somewhat arbitrary, heuristic operation. Table 1 lists parameters assigned in previous works (Guzzetti et al., 2003, 2004). Values of the coefficients, in the model, depend only on the soil type existing in the slope. For this reason, one can safely extract values of the parameters that have proven effective by Guzzetti et al. (2003, 2004), for similar soil types. For our study, we used values for the energy restitution and dynamic friction parameters taken from Guzzetti et al. (2004) for the “talus” and “landslide deposits”, whereas for the rockslide scarp area (Fig. 1B) an average value between those adopted for the “landslide scar” by Guzzetti et al. (2003) and “landslide crown area” by Guzzetti et al. (2004) was chosen (Table 1). We considered a 5% variation range of the values of the restitution coefficients and dynamical friction angle around the values obtained from the literature; the code samples randomly the values of such parameters within the given range, within each corresponding terrain type, for each simulated trajectory.

#### 4 Results and discussion

Figure 3 shows a map of the locations of the rockfall source areas (Fig. 3A), and the grid with the trajectory count for each cell obtained by STONE (Fig. 3B), together with the location of the rockfalls triggered by the seismic sequence that were observed in the field (red triangles). From the 318 source area cells, it was simulated a total of 31,800 rockfall trajectories (i.e., 100 simulations per source cell), 25,845 of which overlap at least once over the study area. The trajectories affect an area of 39,561 cells ( $m^2$ ), and the count of the trajectories spans between 1 and 710, with a mean of 26.5 (median = 9, standard deviation = 43.4).

Inspection of Figure 3B reveals that the modelled rockfall trajectories can reach the SP18 in several sites. In particular, in Figure 3B the black dashed lines identify the portion of the road most affected by rockfall trajectories, as opposed to the remaining part of the road. This is consistent with field observations (Fig. 3B). The portion of the SP18 closest to the rockfall source site S1 was not hit by the rockfalls during the seismic sequence, and it is interested overall by a total 33 pixels showing a value of 1 within the road or downhill of it. This represents 0.01% of the total number of simulated rockfall trajectories and were consequently considered negligible. On the contrary, the portion of the SP18 downhill of S2, and which was hit by the rockfall during the seismic sequence, is correctly predicted by the model as subject to rockfall hazard. In detail, the model output identifies a total of 5,108 trajectories crossing the road; 16% of the simulated trajectories. Local values reaching 140 trajectories were identified downhill of S2. Figure 3C shows the number of trajectories reaching the SP18 and.

[FIGURE 3]



The workflow described in this paper for the assessment of the road exposure to rockfall hazard was carried out during a seismic emergency phase to support the Italian National Department of Civil Protection in the decision whether or not to safely reopen the SP18 road to traffic. The diffuse presence of trees in the study area would have required a LiDAR survey to collect ground elevation data under the trees canopy. However, since the seismic emergency framework imposed a strict time constraint, a LiDAR acquisition was ruled out since it would have required a long planning, preparation and post-processing time compared to other techniques. Among the existing photogrammetric acquisition approaches, use of RPAS is the easiest to plan and carry out, and it is one of the most widespread and used also in the private professional sector. From the methodological point of view, the application described in this study can be considered as a procedure, applicable during emergencies, for the acquisition of all the required elements that can support the implementation of numerical models for rockfall hazard and risk assessment at a relatively low cost. For areas up to few tens of square kilometres, the use of RPAS is the cheapest and fastest method for the acquisition of orthophotos and DSMs but, on the other hand, vegetation hampers the quality of the resulting DTMs, fundamental to obtain reliable numerical rockfall simulations. To overcome this limitation, integration of aerial imagery with GNSS RTK points measured in the field is mandatory for accurate mapping applications, especially when the accuracy required as input by the numerical model is not very high. The availability of ultra-high resolution images can be very useful for the delineation of rockfall source areas, one of the inputs required by numerical modelling.

The results of STONE are influenced by the values of the tangential and normal restitution and dynamical friction coefficient, which are assigned based on the characterization of the land cover, in most cases accomplished by geomorphological mapping (Fig. 1B). In this case, the detailed geomorphological mapping was carried out based on a rigid set of rules and criteria that make it repeatable and less subjective (Santangelo et al., 2015a, b; Fiorucci et al., 2018). To prove the influence of the detail of the geomorphological mapping on the results, we run STONE assigning the parameters generalizing the initial geomorphological map, considering the entire scarp of the rockslide as a talus, instead of distinguishing the three smaller talus deposits in the same slope. Results showed that, assigning the parameters based on a generalized version of the geomorphological map results in trajectories that do not reproduce the location of the boulders observed in the field. This is consistent with the relatively larger value of the friction coefficient ascribed to “talus” than the “landslide scarp” one (Guzzetti et al., 2004, Table 1). Such an evidence shows that the quality of the geomorphological mapping (Guzzetti et al., 2012) has a relevant effect on model results. The rockfall simulation prepared by STONE confirmed that the portion of the SP18 road affected by the rockfall is rather limited (Fig. 3C). During the emergency phase, this information was provided to the National Department of Civil Protection to support the decision about the road reopening conditions. It was advised that the road could be safely reopened to the traffic, provided that (i) protection measures were installed above the SP18 road where the model indicated the exposure of the road to rockfall trajectories, and (ii) that the rockfall barriers installed should take into account the size of the boulders recognized in the field.

Modelling results show that outside the most hazardous part of the SP18 (Fig. 3B, C), only few locations are potentially affected by rockfalls. Here, the 33 trajectories that could potentially reach the road show count values of one. It is worth noting that, over 100 trajectories simulations for each source pixel, a count value of one suggests a probability of occurrence that is equal to  $1 \times 10^{-2}$ . It actually corresponds to probability values much smaller since most frequently a single pixel can be



crossed by trajectories starting from different (even not so close) locations. In the case of the tract of the road threatened by the site S1, the total number of simulated trajectories that could reach the road represented the 0.01% of the total. This estimate was obtained by counting the number of pixels used as source area located uphill of the road in S1 and the total number of trajectories that reached the road. Such a method represents a semi-quantitative estimate. Like other rockfall modeling software, STONE outputs a frequency map, whereas the evaluation of the probability of rockfall represents still an open problem due to the presence of the pixels where modelled trajectories overlap with others modelled from other source areas. Hence, a rigorous probabilistic estimation would require that each trajectory should be modelled keeping track of the source area. Possible future development of STONE or similar rockfall models should be able to define a probability value, which would allow better comparing the rockfall hazard conditions in different areas.

STONE does not take into account the vegetation effect although, in this case, the presence of a thick wooded area at the foot of the slope acts as a natural rockfall attenuator between the source areas and the road. As already pointed out by Guzzetti et al. (2004), despite the rockfall modelling is aimed at describing possible rockfall scenarios given the current state of the places, it appears poorly precautionary to consider the barrier effect of the trees in the final assessment. Future wildfires could leave unprotected the road, causing an increase of the overall rockfall hazard.

A non-negligible point of discussion consists in the *caveats* that should be taken into account when using model outputs that contain sources of uncertainty at some step of the procedure, to support decision-making. In this case, for instance, it was acquired a DSM at 20 cm GSD, which is inhomogeneous across the study area due to the presence of the trees canopy. The entire DSM was resampled at 1 m GSD, which is the minimum working resolution of the model STONE, and a reasonable resolution able to capture micro-morphological features, and portray the general morphology reconstructed under the trees canopy by the GNSS-RTK survey. Despite the average GNSS point density is one point per 100 m<sup>2</sup>, the acquisition was planned to best represent the ground morphology, which is characterized by a series of two scarps and counter-escarpments probably built during the quarry exploitation. In our case, it was not possible to obtain a better acquisition because of the following practical limitations: (i) the GNSS signal under the trees canopy was unstable, hence almost every measure had to be repeated several times to get the minimum required accuracy of one meter; and (ii) also the GPRS signal was poor, causing several interruptions in the RTK connection. For these reasons, when acquiring such data in the field, it is advised to collect as many data points as possible. Moreover, in places where the environmental conditions are unfavourable, acquisition should be performed to catch the most representative morphological features.

The overall cost of the materials (i.e., the RPAS, software licenses, GNSS receiver) used in our test case totalled about 23,000 euros, which is a considerably less than a LiDAR acquisition at a comparable resolution. The time required to carry out the entire procedure was estimated in about 15 working days of one person, including the initial survey, the RPAS and the GNSS acquisitions, the photogrammetric processing and the DSM filtering, the integration of the RPAS DSM and the GNSS data points. Despite the overall procedure is not low cost, it is cheaper than a similar procedure involving the use of a LiDAR acquisition instead of an RPAS photogrammetric survey.



## 5 Conclusions

The study described in the article, was conducted during the seismic sequence that hit Central Italy in the period between 24 August 2016 and January 2017 to support the National Department of Civil Protection to identify the conditions to safely reopen the road exposed to rockfalls. The study consisted in the application of a rockfall numerical model (STONE) prepared using a Digital Terrain Model generated by the integration of a DTM obtained by photogrammetry applied to a Remotely Piloted Aerial System (RPAS) acquisition and a GNSS-RTK (Global Navigation Satellite System in Real Time Kinematic mode) survey in densely vegetated areas. The numerical model allowed performing a semi-quantitative evaluation of the residual rockfall risk posed to the road SP18. It was observed that the tract of the road that had been hit by a rockfall during the seismic emergency was predicted as unsafe by the model, since the 16% of the total 31,800 simulated trajectories reached the road. The remaining portion of the studied tract of the SP18 was reached by the 0.01% of the modelled trajectories, and hence its exposure to rockfall was considered negligible.

The described procedure is general and can be successfully applied during emergency phases and in mountainous regions like the study area. The complete photogrammetry-based procedure described in the paper was carried out in a total of 15 working days of one person at an overall cost of 23,000 euros. Considered all the working phases, it is faster and cheaper than LiDAR surveys, and has less logistic constrains. It also allows acquiring denser points clouds compared to LiDAR. On the other hand, it is limited by high vegetation cover. The GNSS-RTK survey can partially solve this limitation, but it is important to know that the final DTM has different quality under the trees canopies and on bare areas.

STONE fails to reproduce the position of the boulders actually fallen during the seismic sequence if parameters are assigned based on generalized geomorphological maps of the covers. Therefore, it is advised that the quality of the input geomorphological mapping be as high as possible, and compatible with the resolution of the input DEM.

*Author contributions.* MS contributed to the field survey and the geomorphological mapping, acquired the GNSS-RTK data, analyzed the results, and wrote the text. MA run the model STONE, and contributed to writing the paper. MB acquired and processed the RPAS data. MC contributed to the geomorphological mapping, and reviewed the text. DG acquired and processed the RPAS data, analyzed the results, and contributed to writing the text. FG contributed to the field survey and reviewed the text. IM acquired the GNSS-RTK data, analyzed the results, and contributed to writing the text. PR reviewed the text.

*Competing interests.* The authors declare no competing interests

*Disclaimer.* In this work, use of copyright, brand, trade names, and logos is for descriptive and identification purposes only, and does not imply endorsement from the authors, or their institutions.



*Acknowledgements.* The work was partly funded by the Italian National Department of Civil Protection.



## References

- Agliardi, F. and Crosta, G. B.: High resolution three-dimensional numerical modelling of rockfalls, *International Journal of Rock Mechanics & Mining Sciences*, 40, 455–471, [https://doi.org/10.1016/S1365-1609\(03\)00021-2](https://doi.org/10.1016/S1365-1609(03)00021-2), [https://ac.els-cdn.com/S1365160903000212/1-s2.0-S1365160903000212-main.pdf?{}\\_tid=46d4e891-e66e-4d42-9665-fd274f5bba1d&{}acdnat=1528992171{ }6c150bd206942cec3e4d95b4850c0825](https://ac.els-cdn.com/S1365160903000212/1-s2.0-S1365160903000212-main.pdf?{}_tid=46d4e891-e66e-4d42-9665-fd274f5bba1d&{}acdnat=1528992171{ }6c150bd206942cec3e4d95b4850c0825), 2003.
- 5 Boccardo, P., Chiabrando, F., Dutto, F., Tonolo, F., and Lingua, A.: UAV Deployment Exercise for Mapping Purposes: Evaluation of Emergency Response Applications, *Sensors*, 15, 15 717–15 737, <https://doi.org/10.3390/s150715717>, <http://www.mdpi.com/1424-8220/15/7/15717>, 2015.
- Budetta, P.: Assessment of rockfall risk along roads, *Natural Hazards and Earth System Sciences*, 4, 71–81, <https://www.nat-hazards-earth-syst-sci.net/4/71/2004/nhess-4-71-2004.pdf>, 2004.
- 10 Cacciuni, A., Centamore, E., Di Stefano, R., and F. D.: Evoluzione morfotettonica della conca di Amatrice, *Studi Geologici Camerti*, spec 1995/2, 95–100, 1995.
- Chou, T.-Y., Yeh, M.-L., Chen, Y.-C., and Chen, Y.-H.: Disaster monitoring and management by the unmanned aerial vehicle technology, in: *ISPRS TC VII Symposium – 100 Years ISPRS*, edited by Wagner W., Székely, B., pp. 137–142, Vienna, <http://www.isprs.org/proceedings/xxxviii/part7/b/pdf/137{ }XXXVIII-part7B.pdf>, 2010.
- 15 Corominas, J., Copons, R., Moya, J., Vilaplana, J. M., Altimir, J., and Amigó, J.: Quantitative assessment of the residual risk in a rockfall protected area, *Landslides*, 2, 343–357, <https://doi.org/10.1007/s10346-005-0022-z>, <http://link.springer.com/10.1007/s10346-005-0022-z>, 2005.
- Evans S, G.: Fatal landslides and landslide risk in Canada, in: *Landslide Risk Assessment*, edited by Cruden D, F. R., pp. 186–196, Balkema, Rotterdam, 1997.
- 20 Ezequiel, C. A. F., Cua, M., Libatique, N. C., Tangonan, G. L., Alampay, R., Labuguen, R. T., Favila, C. M., Honrado, J. L. E., Canos, V., Devaney, C., Loreto, A. B., Bacusmo, J., and Palma, B.: UAV aerial imaging applications for post-disaster assessment, environmental management and infrastructure development, in: *2014 International Conference on Unmanned Aircraft Systems (ICUAS)*, pp. 274–283, IEEE, <https://doi.org/10.1109/ICUAS.2014.6842266>, <http://ieeexplore.ieee.org/document/6842266/>, 2014.
- 25 Ferlisi, S., Cascini, L., Corominas, J., and Matano, F.: Rockfall risk assessment to persons travelling in vehicles along a road: the case study of the Amalfi coastal road (southern Italy), *Natural Hazards*, 62, 691–721, <https://doi.org/10.1007/s11069-012-0102-z>, <http://link.springer.com/10.1007/s11069-012-0102-z>, 2012.
- Fiorucci, F., Giordan, D., Santangelo, M., Dutto, F., Rossi, M., and Guzzetti, F.: Criteria for the optimal selection of remote sensing optical images to map event landslides, pp. 405–417, <https://doi.org/10.5194/nhess-18-405-2018>, [https://www.nat-hazards-earth-syst-sci.net/18/405/2018/](https://www.nat-hazards-earth-syst-sci.net/18/405/2018/nhess-18-405-2018.pdf), 2018.
- 30 Giordan, D., Manconi, A., Facello, A., Baldo, M., Dell’Anese, F., Allasia, P., and Dutto, F.: Brief Communication: The use of an unmanned aerial vehicle in a rockfall emergency scenario, *Natural Hazards and Earth System Science*, 15, 163–169, <https://doi.org/10.5194/nhess-15-163-2015>, <http://www.nat-hazards-earth-syst-sci.net/15/163/2015/>, 2015a.
- Giordan, D., Manconi, A., Tannant, D. D., and Allasia, P.: UAV: Low-cost remote sensing for high-resolution investigation of landslides, in: *2015 IEEE International Geoscience and Remote Sensing Symposium (IGARSS)*, pp. 5344–5347, IEEE, <https://doi.org/10.1109/IGARSS.2015.7327042>, <http://ieeexplore.ieee.org/document/7327042/>, 2015b.
- 35



- Giordan, D., Hayakawa, Y., Nex, F., Remondino, F., and Tarolli, P.: Review article: the use of remotely piloted aircraft systems (RPASs) for natural hazards monitoring and management, *Natural Hazards and Earth System Sciences*, 18, 1079–1096, <https://doi.org/10.5194/nhess-18-1079-2018>, <https://www.nat-hazards-earth-syst-sci.net/18/1079/2018/nhess-18-1079-2018.pdf><https://www.nat-hazards-earth-syst-sci.net/18/1079/2018/>, 2018.
- 5 GRASS Development Team: Geographic Resources Analysis Support System (GRASS GIS) Software, Version 7.2, Open Source Geospatial Foundation, <http://grass.osgeo.org>, 2017.
- Guzzetti, F., Crosta, G., Detti, R., and Agliardi, F.: STONE: a computer program for the three-dimensional simulation of rock-falls, *Computers & Geosciences*, 28, 1079–1093, [https://doi.org/10.1016/S0098-3004\(02\)00025-0](https://doi.org/10.1016/S0098-3004(02)00025-0), <http://linkinghub.elsevier.com/retrieve/pii/S0098300402000250>, 2002.
- 10 Guzzetti, F., Reichenbach, P., and Wieczorek, G. F.: Rockfall hazard and risk assessment in the Yosemite Valley, California, USA, *Natural Hazards and Earth System Sciences*, 3, 491–503, <https://www.nat-hazards-earth-syst-sci.net/3/491/2003/nhess-3-491-2003.pdf>, 2003.
- Guzzetti, F., Reichenbach, P., and Ghigi, S.: Rockfall hazard and risk assessment along a transportation corridor in the Nera Valley, central Italy., *Environmental management*, 34, 191–208, <http://www.ncbi.nlm.nih.gov/pubmed/15559944>, 2004.
- Guzzetti, F., Mondini, A. C., Cardinali, M., Fiorucci, F., Santangelo, M., and Chang, K.-T.: Landslide inventory maps: New tools for an old
- 15 problem, *Earth-Science Reviews*, 112, 42–66, <https://doi.org/10.1016/j.earscirev.2012.02.001>, <http://linkinghub.elsevier.com/retrieve/pii/S0012825212000128>, 2012.
- Huang, H., Long, J., Yi, W., Yi, Q., Zhang, G., and Lei, B.: A method for using unmanned aerial vehicles for emergency investigation of single geo-hazards and sample applications of this method, *Hazards Earth Syst. Sci.*, 17, <https://doi.org/10.5194/nhess-17-1961-2017>, <https://doi.org/10.5194/nhess-17-1961-2017>, 2017.
- 20 Jaboyedoff, M. and Labiouse, V.: Technical Note: Preliminary estimation of rockfall runout zones, *Nat. Hazards Earth Syst. Sci.*, 11, 819–828, <https://doi.org/10.5194/nhess-11-819-2011>, [www.nat-hazards-earth-syst-sci.net/11/819/2011/](http://www.nat-hazards-earth-syst-sci.net/11/819/2011/), 2011.
- Liu, C.-C., Chen, P.-L., Matsuo, T., and Chen, C.-Y.: Rapidly responding to landslides and debris flow events using a low-cost unmanned aerial vehicle, *Journal of Applied Remote Sensing*, 9, 096 016, <https://doi.org/10.1117/1.JRS.9.096016>, <http://remotesensing.spiedigitallibrary.org/article.aspx?doi=10.1117/1.JRS.9.096016>, 2015.
- 25 Luuk Dorren, A. K.: Rockyfor3D (v5.2) revealed - Transparent description of the complete 3D rockfall model, *ecorisQ papers*, pp. 1–37, [https://www.ecorisq.org/docs/Rockyfor3D{v5}\\_{2}\\_{EN}.pdf](https://www.ecorisq.org/docs/Rockyfor3D{v5}_{2}_{EN}.pdf), 2015.
- Michoud, C., Derron, M.-H., Horton, P., Jaboyedoff, M., Baillifard, F.-J., Loye, A., Nicolet, P., Pedrazzini, A., and Queyrel, A.: Rockfall hazard and risk assessments along roads at a regional scale: example in Swiss Alps, *Nat. Hazards Earth Syst. Sci.*, 12, 615–629, <https://doi.org/10.5194/nhess-12-615-2012>, [www.nat-hazards-earth-syst-sci.net/12/615/2012/](http://www.nat-hazards-earth-syst-sci.net/12/615/2012/), 2012.
- 30 Nex, F. and Remondino, F.: UAV for 3D mapping applications: a review, *Applied Geomatics*, 6, 1–15, <https://doi.org/10.1007/s12518-013-0120-x>, <http://link.springer.com/10.1007/s12518-013-0120-x>, 2014.
- Obanawa, H. Hayakawa, Y. and Gomez, C.: 3D Modelling of Inaccessible Areas using UAV-based Aerial Photography and Structure from Motion, *Transactions, Japanese Geomorphological Union*, 35, 283–294, <https://www.researchgate.net/publication/261724285>, 2014.
- Razak, K. A., Santangelo, M., Van Westen, C. J., Straatsma, M. W., and de Jong, S. M.: Generating an optimal DTM
- 35 from airborne laser scanning data for landslide mapping in a tropical forest environment, *Geomorphology*, 190, 112–125, <https://doi.org/10.1016/j.geomorph.2013.02.021>, <http://linkinghub.elsevier.com/retrieve/pii/S0169555X13001086>, 2013.
- Salvini, R., Mastrorocco, G., Seddaiu, M., Rossi, D., and Vanneschi, C.: The use of an unmanned aerial vehicle for fracture mapping within a marble quarry (Carrara, Italy): photogrammetry and discrete fracture network modelling The use of an unmanned aerial vehicle for fracture



- mapping within a marble quarry (Carrara, Italy): photogrammetry and discrete fracture network modelling, *Geomatics, Natural Hazards and Risk*, 8, 34–52, <https://doi.org/10.1080/19475705.2016.1199053>, <http://www.tandfonline.com/action/journalInformation?journalCode=tgnh20>, 2016.
- 5 Salvinì, R., Mastroiocco, G., Esposito, G., Di Bartolo, S., Coggan, J., and Vanneschi, C.: Use of a remotely piloted aircraft system for hazard assessment in a rocky mining area (Lucca, Italy), *Hazards Earth Syst. Sci.*, 18, 287–302, <https://doi.org/10.5194/nhess-18-287-2018>, 2018.
- Santangelo, M., Gioia, D., Cardinali, M., Guzzetti, F., and Schiattarella, M.: Landslide inventory map of the upper Sinni River valley, Southern Italy, *Journal of Maps*, 11, 444–453, <https://doi.org/10.1080/17445647.2014.949313>, <http://dx.doi.org/10.1080/17445647.2014.949313>, <http://www.tandfonline.com/doi/abs/10.1080/17445647.2014.949313>, <https://www.tandfonline.com/doi/full/10.1080/17445647.2014.949313>, 2015a.
- 10 Santangelo, M., Marchesini, I., Bucci, F., Cardinali, M., Fiorucci, F., and Guzzetti, F.: An approach to reduce mapping errors in the production of landslide inventory maps, *Natural Hazards and Earth System Sciences*, 15, 2111–2126, <https://doi.org/10.5194/nhess-15-2111-2015>, 2015b.
- Saroglou, C., Asteriou, P., Zekkos, D., Tsiambaos, G., Clark, M., and Manousakis, J.: UAV-based mapping, back analysis and trajectory modeling of a coseismic rockfall in Lefkada island, Greece, *Hazards Earth Syst. Sci.*, 18, 321–333, <https://doi.org/10.5194/nhess-18-321-2018>, 2018.
- 15 Török, Á., Barsi, Á., Bögöly, G., Lovas, T., Somogyi, Á., and Görög, P.: Slope stability and rockfall assessment of volcanic tuffs using RPAS with 2-D FEM slope modelling, *Hazards Earth Syst. Sci.*, 18, 583–597, <https://doi.org/10.5194/nhess-18-583-2018>, <https://www.nat-hazards-earth-syst-sci.net/18/583/2018/nhess-18-583-2018.pdf>, 2018.
- 20 Turner, D., Lucieer, A., and Watson, C.: An Automated Technique for Generating Georectified Mosaics from Ultra-High Resolution Unmanned Aerial Vehicle (UAV) Imagery, Based on Structure from Motion (SfM) Point Clouds, *Remote Sensing*, 4, 1392–1410, <https://doi.org/10.3390/rs4051392>, <http://www.mdpi.com/2072-4292/4/5/1392>, 2012.
- van Dijke, J. J. and van Westen, C. J.: Rockfall hazard : a geomorphologic application of neighbourhood analysis with ILWIS, *International journal of applied earth observation and geoinformation*, pp. 40–44, 1990.
- 25 Westoby, M. J., Brasington, J., Glasser, N. F., Hambrey, M. J., and Reynolds, J. M.: ‘Structure-from-Motion’ photogrammetry: A low-cost, effective tool for geoscience applications, *Geomorphology*, 179, 300–314, <https://doi.org/10.1016/J.GEOMORPH.2012.08.021>, <https://www.sciencedirect.com/science/article/pii/S0169555X12004217>, 2012.
- Whalley W, B.: Rockfalls, in: *Slope Stability*, edited by Cruden D, F. R., pp. 217–256, Wiley, New York, 1984.
- Xu, Z., Yang, J., Peng, C., Wu, Y., Jiang, X., Li, R., Zheng, Y., Gao, Y., Liu, S., and Tian, B.: Development of an UAS for post-earthquake disaster surveying and its application in Ms7.0 Lushan Earthquake, Sichuan, China, *Computers & Geosciences*, 68, 22–30, <https://doi.org/10.1016/j.cageo.2014.04.001>, <http://linkinghub.elsevier.com/retrieve/pii/S0098300414000788>, 2014.

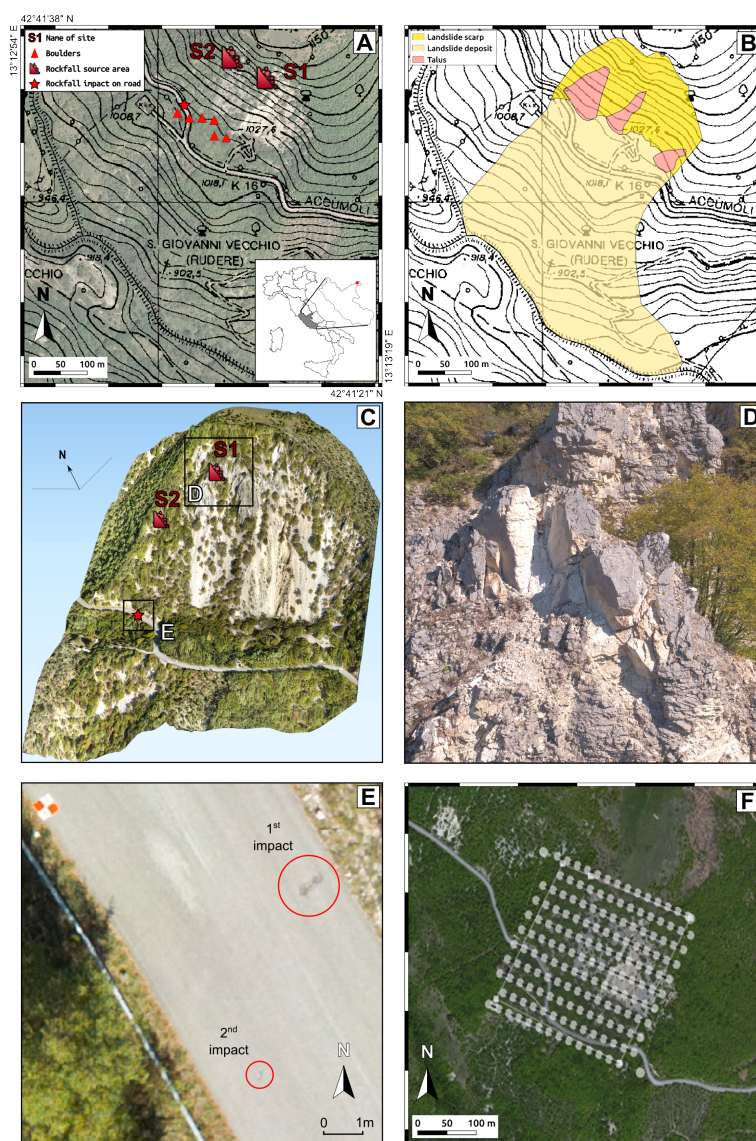


**Figure 1.** Location of the study area. (A) Topographic map: Carta Tecnica Regionale of the Lazio Region, at 1:10,000 scale. Colour orthophoto map: AGEA (2012). Symbols named as S1 and S2 indicate the source areas of the fallen boulders. Red star shows location where a boulder hit and crossed the SP18 road. Red triangles indicate the boulders found at the farthest locations from the source areas along the talus slope during the field survey. (B) Map of surface deposits obtained through the visual interpretation of the available aerial photographs. (C) 3D perspective of the study area. Image base and elevation data were obtained ad hoc through a RPAS flight flown on 10 October 2016. (D) S1 rockfall source area. Oblique photograph taken by the RPAS. (E) Detail of the orthophotograph obtained by the RPAS showing impact points of the boulder detached from the S2 source area. (F) Flight plan of the multicopter for the acquisition of aerial photographs.

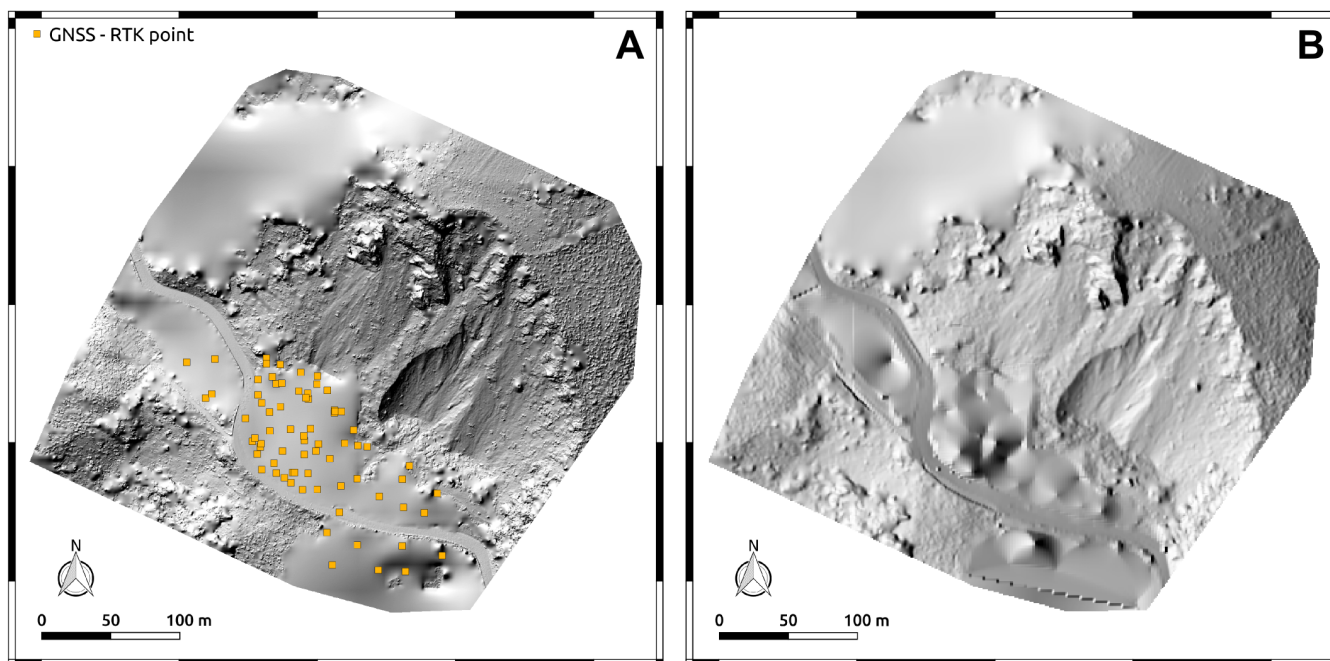


**Figure 2.** Shaded relief images of the study area. (A) Image prepared using the DTM obtained with the photogrammetric procedure, after vegetation filtering. (B) Image prepared integrating the GNSS-RTK data points (yellow squares in A) with the DTM. DTM shown in (B) was resampled at a resolution of  $1\text{ m} \times 1\text{ m}$ , for modelling purposes.

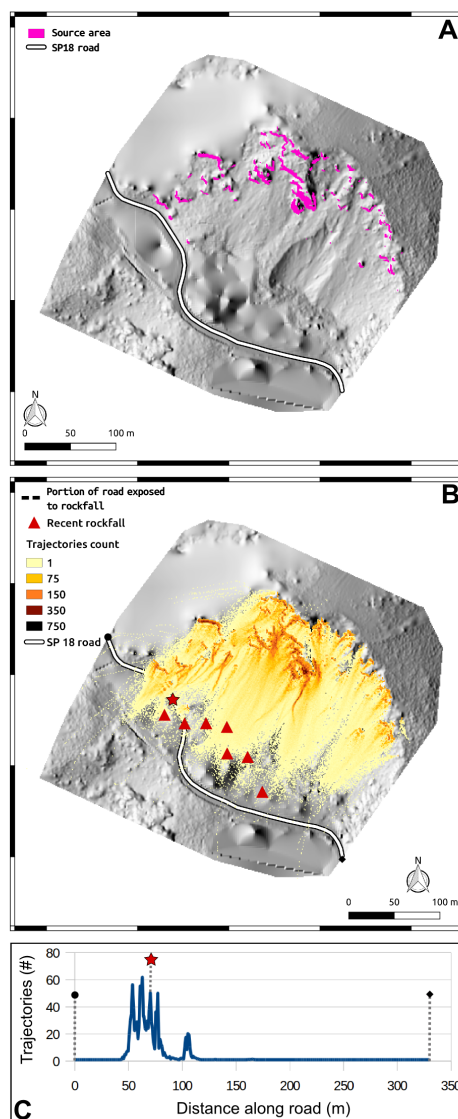


**Figure 3.** (A) Location of rockfall source areas (pink). Background image is the shaded relief map obtained from the  $1\text{ m} \times 1\text{ m}$  DSM calculated from aerial images and integrated with GPS-RTK measurements (Fig. 2). (B) STONE simulation output. The map shows the number of trajectories for each cell. Red triangles represent large boulders observed during the field survey at their farthest locations from the source areas. The red star indicates the position of the impact point found on the SP18. (C) Count of simulated rockfall trajectories along the SP18 road. The circle and the diamond indicate start and end point of the road profile. The red star indicates the position of the impact point found on the SP18.



**Table 1.** Values of the dynamic rolling friction angle and of the normal and tangential energy restitution coefficients assigned to different terrain types in the literature, and used in this work.

Terrain type	Rolling friction	Normal restitution	Tangential restitution
<i>Guzzetti et al. (2003)</i>			
Recent debris flow	0.65	30	50
Recent rock fall and rock slide	0.75	35	55
Rock fall path	0.30	65	80
Landslide scar*	0.20	65	80
Historical debris slide	0.60	30	55
Historical rock fall and rock slide	0.75	40	60
Prehistorical debris flow	0.60	35	60
Prehistorical rock fall and rock slide	0.70	35	55
Prehistorical rock avalanche	0.60	40	60
Talus deposit	0.70	35	55
Bedrock	0.30	65	80
Alluvial deposit	0.85	15	20
<i>Guzzetti et al. (2004)</i>			
Alluvial deposit	0.80	15	30
Alluvial fan	0.60	25	55
Debris cone	0.60	30	50
Debris deposit	0.70	35	55
Shallow debris deposit	0.70	35	60
Talus **	0.65	35	55
Landslide deposit ***	0.40	45	55
Landslide crown area*	0.35	55	65
Debris flow deposit	0.65	30	55
Debris flow source area	0.55	35	60
Massive and thickly layered limestone and Travertine deposit	0.30	65	75
Rockfall source area in massive and thickly layered limestone, and Travertine deposit	0.25	65	75
Thinly bedded limestone, cherty limestone	0.35	60	70
Marly limestone, marl and clay	0.40	55	65
Rockfall source area in marly limestone, marl and clay	0.35	55	65
<i>This study</i>			
Landslide scarp *	0.30	65	80
Talus **	0.65	35	55
Landslide deposit ***	0.40	45	55